

## Alizarin red: An efficient Inhibitor of C38 Steel Corrosion in Hydrochloric Acid

D. Ben Hmamou<sup>1</sup>, R. Salghi<sup>1,\*</sup>, A. Zarrouk<sup>2</sup>, H. Zarrok<sup>3</sup>, B. Hammouti<sup>2</sup>, S. S. Al-Deyab<sup>4</sup>, M. Bouachrine<sup>5</sup>, A. Chakir<sup>6</sup>, M. Zougagh<sup>7</sup>

<sup>1</sup> Equipe de Génie de l'Environnement et de Biotechnologie, ENSA, Université Ibn Zohr, BP 1136 Agadir, Morocco

<sup>2</sup> LCAE-URAC18, Faculté des Sciences, Université Mohammed Premier, BP 4808, Oujda, Morocco.

<sup>3</sup> Laboratoire des procédés de séparation, Faculté des Sciences, Kénitra, Morocco

<sup>4</sup> Petrochemical Research Chair, Department of Chemistry - College of Science, King Saud University, B.O. 2455 Riaydh 11451 Saudi Arabia.

<sup>5</sup> ESTM, Université Moulay Ismail, Meknes, Maroc.

<sup>6</sup> GSMA, UMR CNRS 6089, Faculté des Sciences, université de Reims, UMR 6089,

<sup>7</sup> Regional Institute for Applied Science Research, IRICA, E-13004 Ciudad Real, Spain

\*E-mail: [r\\_salghi@yahoo.fr](mailto:r_salghi@yahoo.fr)

Received: 4 April 2012 / Accepted: 18 May 2012 / Published: 1 June 2012

---

Corrosion inhibition efficiency of alizarin red (AZR) as corrosion inhibitor on C38 steel in acid solution was investigated by means of weight loss, potentiodynamic polarization curve, electrochemical impedance spectroscopy (EIS) and Quantum chemical method. The inhibition efficiency was found to increase with increase in AZR concentration but decreased temperature. Weight loss measurements gave an inhibition efficiency of about 65.8 % in the presence of  $1 \times 10^{-5}$  M alizarin red, which increased to about 96.3 % at AZR concentration of  $1 \times 10^{-2}$  M. EIS results revealed that alizarin red took effects excellently as a corrosion inhibitor for C38 steel in 1 M hydrochloric acid media, and its efficiency attains more than 96.5% at  $1 \times 10^{-2}$  M at 298 K. Changes in impedance parameters (charge transfer resistance,  $R_{ct}$ , and double layer capacitance,  $C_{dl}$ ) were indicative of adsorption of AZR on the C38 steel surface, leading to the formation of protective films. Potentiodynamic polarization measurements showed that the presence of AZR in 1 M hydrochloric acid solutions decreased corrosion currents to a great extent. The above results showed that AZR acted as a mixed-type corrosion inhibitor. The adsorption of used compound on the steel surface obeys Langmuir's isotherm. The apparent activation energie, enthalpie and entropie of the dissolution process and the free energie were determined and discussed. The correlation between the inhibition efficiency and quantum chemical parameters was investigated in order to elucidate the inhibition mechanism of the investigated compound.

---

**Keywords:** C38 Steel; HCl; Inhibition; Alizarin Red; Weight Loss; Electrochemical Polarization ; EIS; DFT.

## 1. INTRODUCTION

Steel is widely used in most industries because of its low cost and availability for the manufacture of reaction vessels such as cooling tower reservoirs, pipelines, etc. [1]. Corrosion is a fundamental process playing an important role in economics and safety, particularly for metals and alloys. Acid solutions are used in industry to remove mill scale from metallic surfaces [2–3]. Because of the general aggression of acid solutions, inhibitors are commonly used to reduce the corrosive attack on metallic materials. The effect of organic nitrogen compounds on the corrosion behaviour of metallic materials in aggressive solutions has been well documented [4–23]. Their adsorption characteristics depend on several factors including the nature and number of potential adsorption sites present in the dye molecule. Among these wide use of inhibitors, Alizarin violet was successively used as inhibitor of steel corrosion in HCl and H<sub>2</sub>SO<sub>4</sub> solutions [24,25].

In this work, alizarin red had been studied on the corrosion inhibition of C38 steel in 1M HCl solutions by weight loss, electrochemical methods and Theoretical Studies. Also, the kinetics of corrosion of steel in acid medium has been identified by electrochemical impedance spectroscopy method. The correlation between the inhibition efficiency and quantum chemical parameters was investigated in order to elucidate the inhibition mechanism of the investigated compound.

Figure 1 shows the molecular structure of the investigated compound. The presence of oxygen and the electron cloud on the aromatic nucleus suggests that alizarin red should be a good corrosion inhibitor.

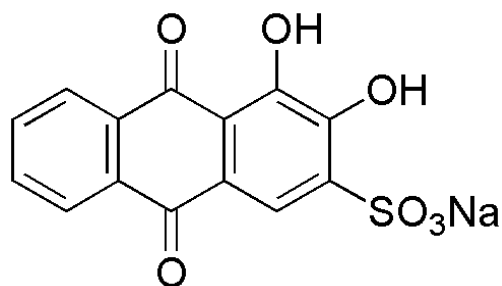


**Figure 1.** The molecular structure of alizarin red.

## 2. MATERIALS AND METHODS

### 2.1. Weight loss measurements

Coupons were cut into  $2 \times 2 \times 0.08 \text{ cm}^3$  dimensions having composition (0.179% C, 0.165% Si, 0.439% Mn, 0.203% Cu, 0.034% S and Fe balance) are used for weight loss measurements. Prior to

all measurements, the exposed area was mechanically abraded with 180, 320, 800, 1200 grades of emery papers. The specimens are washed thoroughly with bidistilled water, degreased and dried with ethanol. Gravimetric measurements are carried out in a double walled glass cell equipped with a thermostated cooling condenser. The solution volume is 80 cm<sup>3</sup>. The immersion time for the weight loss is 6 h at 298 K.

## 2.2. Electrochemical tests

The electrochemical study was carried out using a potentiostat PGZ100 piloted by Voltmaster software. This potentiostat is connected to a cell with three electrode thermostats with double wall (Tacussel Standard CEC/TH). A saturated calomel electrode (SCE) and platinum electrode were used as reference and auxiliary electrodes, respectively. The material used for constructing the working electrode was the same used for gravimetric measurements. The surface area exposed to the electrolyte is 0.094 cm<sup>2</sup>.

Potentiodynamic polarization curves were plotted at a polarization scan rate of 0.5 mV/s. Before all experiments, the potential was stabilized at free potential during 30 min. The polarisation curves are obtained from -800 mV to -400 mV at 298 K. The solution test is there after de-aerated by bubbling nitrogen. Gas bubbling is maintained prior and through the experiments. In order to investigate the effects of temperature and immersion time on the inhibitor performance, some test were carried out in a temperature range 298–328 K.

The electrochemical impedance spectroscopy (EIS) measurements are carried out with the electrochemical system (Tacussel), which included a digital potentiostat model Voltalab PGZ100 computer at  $E_{\text{corr}}$  after immersion in solution without bubbling. After the determination of steady-state current at a corrosion potential, sine wave voltage (10 mV) peak to peak, at frequencies between 100 kHz and 10 mHz are superimposed on the rest potential. Computer programs automatically controlled the measurements performed at rest potentials after 0.5 hour of exposure at 298 K. The impedance diagrams are given in the Nyquist representation. Experiments are repeated three times to ensure the reproducibility.

## 2.3. Solutions preparation

The aggressive solution (1 M HCl) was prepared by dilution of Analytical Grade 37 % HCl with distilled water. The organic compound tested is alizarin red. Its molecule formula is shown in Figure 1. The concentration range of this compound was 10<sup>-2</sup> to 10<sup>-5</sup> M.

## 2.4. Quantum chemical calculations

Complete geometrical optimizations of the investigated molecules are performed using DFT (density functional theory) with the Beck's three parameter exchange functional along with the Lee–Yang–Parr nonlocal correlation functional (B3LYP) [26–28] with 6-31G\* basis set is implemented in

Gaussian 03 program package [29]. This approach is shown to yield favorable geometries for a wide variety of systems. This basis set gives good geometry optimizations. The geometry structure was optimized under no constraint. The following quantum chemical parameters were calculated from the obtained optimized structure: the energy of the highest occupied molecular orbital ( $E_{\text{HOMO}}$ ), the energy of the lowest unoccupied molecular orbital ( $E_{\text{LUMO}}$ ),  $\Delta E_{\text{gap}} = E_{\text{HOMO}} - E_{\text{LUMO}}$ , the dipole moment ( $\mu$ ) and total energy (TE).

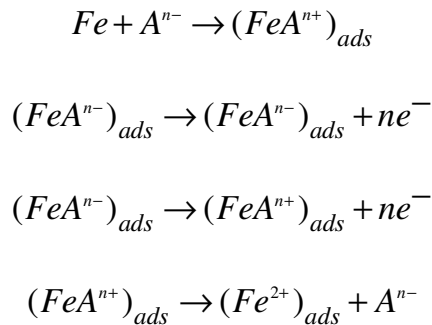
### 3. RESULTS AND DISCUSSION

#### 3.1. Potentiodynamic tests

Polarization measurements have been carried out in order to gain knowledge concerning the kinetics of the anodic and cathodic reactions. The obtained polarization curves of carbon steel in 1M HCl solution without and with different AZR concentrations are shown in Figure 2. The values of the electrochemical kinetic parameters (corrosion potential ( $E_{\text{corr}}$ ), corrosion current density ( $I_{\text{corr}}$ ) and Tafel slopes ( $b_c$ )), determined from these experiments by extrapolation method, are summarized in Table 1. They show that the addition of the inhibitor hindered the acid attack of the carbon steel electrode. The  $I_{\text{corr}}$  values were used to calculate the inhibition efficiency,  $E_I(\%)$  (listed in Table 1), using the following equation [30]:

$$E_I(\%) = \left( \frac{I_{\text{corr}} - I'_{\text{corr}}}{I_{\text{corr}}} \right) \times 100 \quad (1)$$

Where  $I_{\text{corr}}$  and  $I'_{\text{corr}}$  are uninhibited and inhibited corrosion current densities, respectively. Under the experimental conditions performed, the cathodic branch represents the hydrogen evolution reaction, while the anodic branch represents the iron dissolution reaction. They are determined by extrapolation of Tafel lines to the respective corrosion potentials. Some of the authors proposed the following mechanism for the corrosion of iron and steel in acid solution [31–33]:



The cathodic hydrogen evolution

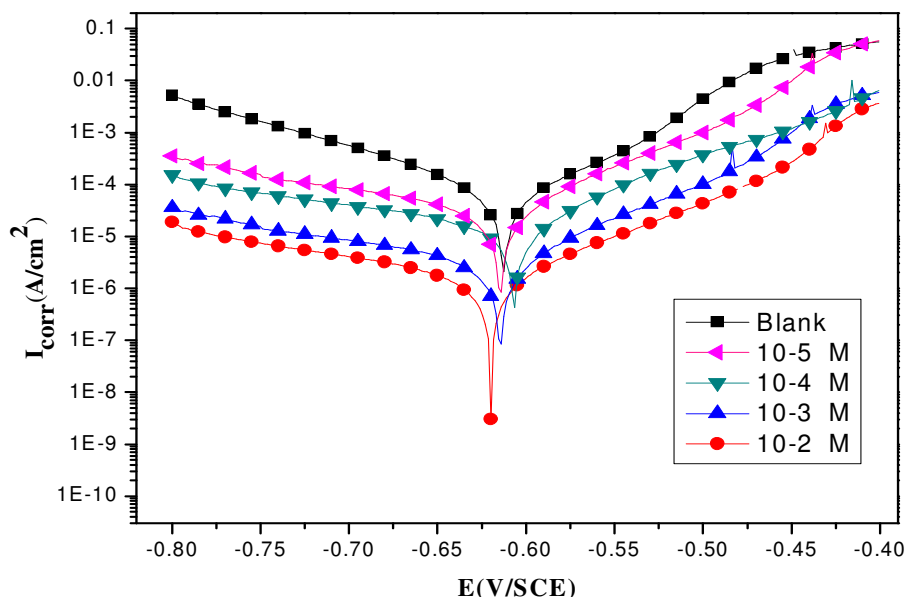
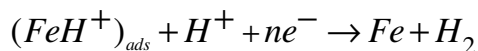
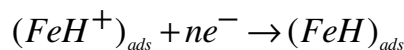
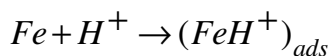


**Figure 2.** Potentiodynamic polarisation curves of steel in 1M HCl in the presence of different concentrations of alizarin red.

**Table 1.** Electrochemical parameters of steel at various concentrations of Alizarin red in 1M HCl and corresponding inhibition efficiency.

Cinh (M)	E <sub>corr</sub> vs. SCE (mV)	I <sub>corr</sub> (µA/cm <sup>2</sup> )	-bc (mV/dec)	EI (%)
Blank	-612	124	149	-
10-5	-614	38	151	69.3
10-4	-606	15	160	87.9
10-3	-613	10	150	91.9
10-2	-533	3	152	97.6

The corrosion potential ( $E_{corr}$ ) in solutions containing inhibitor is shifted towards more positive values with the increase of its concentration (Table 1). Figure 2 indicates that all the cathodic polarization curves are parallel and cathodic Tafel slopes  $bc$  change slightly with increase of AZR concentration, which suggests that the hydrogen evolution is activation controlled and the reduction mechanism is not affected by the presence of the inhibitor [34, 35].

Compared to the blank sample, the anodic curves of the carbon steel electrode in the acid solution shift obviously to the direction of current reduction as adding the AZR, which implies that the organic compounds can also suppress the anodic reaction (steel dissolution) and the variation in the anodic Tafel slope  $b_a$  may be due to the chloride ions/or inhibitor molecules adsorption onto carbon steel surface [36]. Based on the marked decrease of the cathodic and anodic current densities upon introducing the inhibitor in the aggressive solution, this inhibitor is considered as a mixed-type inhibitor. This means that the addition of AZR reduces the anodic dissolution and also retards the cathodic hydrogen evolution reaction.

Differently, for anodic polarization curves with AZR (Figure 2), it seems that when the carbon steel electrode potential is higher than about -300mV/SCE, the presence of the AZR does not change the Figure 2. Polarization curves for carbon steel in 1M HCl containing different concentrations of AZR. current vs. potential characteristics. Such potential can be defined as desorption potential [37, 38]. This phenomenon may be due to desorption of the AZR molecules from the electrode surface leading to the metal dissolution. In this case, the desorption rate of the inhibitor is higher than its adsorption rate, so the corrosion current increases more obviously with rising potential [38, 39]. This result shows that the inhibition effect of this compound depends on the electrode potential. Inspection of these data shows that the addition of AZR inhibits the corrosion process in a wide range of concentrations,

$10^{-5} \text{ M} \leq C_{\text{inh}} \leq 10^{-2} \text{ M}$ . The inhibition efficiency increases with  $C_{\text{inh}}$  reaching its maximum value, 97.6%, at  $10^{-2} \text{ M}$ .

### 3.2. Electrochemical impedance spectroscopy measurements

Figure 3. show the Nyquist plots for C38 steel in 1M HCl solution in the absence and presence of different concentrations of the inhibitor. The obtained Nyquist impedance diagrams in most cases does not show perfect semicircle, generally attributed to the frequency dispersion as a result of roughness and inhomogenates of the electrode surface. The data reveal that, each impedance diagram consists of a large capacitive loop with low frequencies dispersion (inductive arc). This inductive arc is generally attributed to anodic adsorbed intermediates controlling the anodic process [40, 41].

The main parameters deduced from the analysis of Nyquist diagram are:

- The resistance of charge transfer  $R_{ct}$  (diameter of high frequency loop)
- The capacity of double layer  $C_{dl}$  which is defined as:

$$C_{dl} = \frac{1}{2\pi f_{\max} R_{ct}} \quad (2)$$

where,  $f_{\max}$  is the maximum frequency and  $\pi = 3.14$

The surface coverage ( $\theta$ ) and the inhibition efficiency obtained from the impedance measurements are defined by the following relations:

$$\Theta = \left( 1 - \frac{R_{ct}^{\circ}}{R_{ct}} \right) \tag{3}$$

$$\%IE_{R_{ct}} = \left( 1 - \frac{R_{ct}^{\circ}}{R_{ct}} \right) \tag{4}$$

where  $R_{ct}^{\circ}$  and  $R_{ct}$  are the charge transfer resistance in the absence and presence of different concentrations of inhibitor, respectively. Table 2 lists impedance parameters of the Nyquist plots of the alizarin red (AZR) in different concentrations.

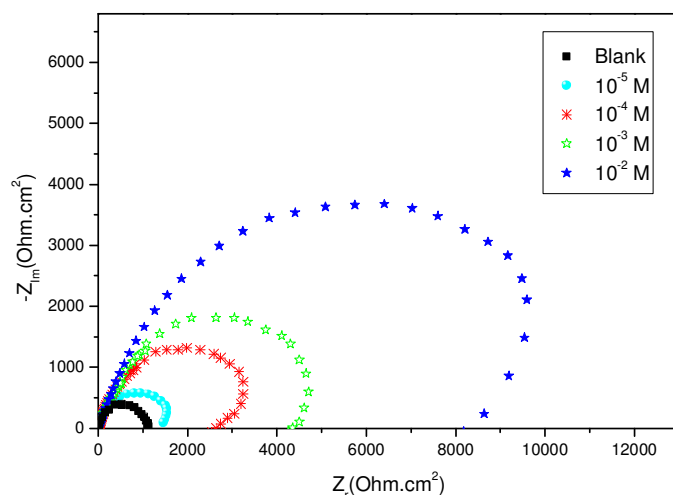


**Figure 3.** Nyquist diagrams for steel electrode with and without Alizarin red after 30 min of immersion.

**Table 2.** Impedance parameters for corrosion of steel in acid at various contents of AZR.

Cinh (M)	Rct (kΩ.cm2)	fmax(Hz)	Cdl (ηF/cm2)	ERct (%)	Θ
Blank	10	50	318	-	-
10-5	31	56	91	67.7	0.677
10-4	96	89	18	89.6	0.896
10-3	110	100	14	90.9	0.909
10-2	286	115	4	96.5	0.965

The Nyquist plots containing depressed semi-circle, whose size increases with the inhibitor concentration represents a charge transfer process mainly controlling the corrosion of C38 steel. It is evident from these plots that the impedance response of mild steel in uninhibited acid solution has significantly changed after the addition of the inhibitor in the aggressive solution. The  $R_{ct}$  values increased with the increasing concentration of the inhibitor indicating that more inhibitor molecule

adsorb on the metal surface at higher concentration and form a protective film on the metal–solution interface [42, 43]. On the other hand, the value of  $C_{dl}$  decreased with increasing inhibitor concentration. Decrease of  $C_{dl}$  may be caused by a reduction in local dielectric constant and/or by an increase in the thickness of the electrical double layer. These results indicate that the inhibitor molecules act by adsorption on the metal/solution interface [44, 45]. These observations suggest that AZR molecule function by adsorption at the metal surface and thereby causing a decrease in the  $C_{dl}$  values and an increase in the  $R_{ct}$  values.

### 3.3. Gravimetric measurements

#### 3.3.1. Effect of concentration

The effect of addition of AZR tested at different concentrations on the corrosion of C38 steel in 1M HCl solution was studied by weight loss measurements at 298 K after 6 h of immersion period. The corresponding data are shown in Table 3. The corrosion rate (W) was calculated from the following equation:

$$W = \frac{(m_1 - m_2)}{(S.t)} \quad (5)$$

where  $m_1$  is the mass of the specimen before corrosion,  $m_2$  the mass of the specimen after corrosion, S the total area of the specimen, t the corrosion time and W the corrosion rate.

With the calculated corrosion rate, the inhibition efficiency of inhibitor for the corrosion of C38 steel was obtained by using the following equation [46]:

$$IE_w(\%) = \left(1 - \frac{W_{corr}}{W_{corr}^{\circ}}\right) \times 100 \quad (6)$$

$W_{corr}$  and  $W_{corr}^{\circ}$  are the corrosion rate of steel samples with and without the inhibitor, respectively.

The degree of surface coverage ( $\Theta$ ) was calculated using equation 7 [46]:

$$\Theta = 1 - \frac{W_{corr}}{W_{corr}^{\circ}} \quad (7)$$

It is obvious from the Table 3 that the AZR inhibit the corrosion of C38 steel in 1 M HCl solution at all concentrations used in this study and the corrosion rate (W) is seen to decrease continuously with increasing additive concentration at 298 K. Indeed, corrosion rate values of mild steel decrease when the inhibitor concentration increases while E (%) values of AZR increase with the increase of the concentration, the maximum E(%) of 98% is achieved at

$10^{-2}$  M. The high inhibitive performance of AZR suggests a higher bonding of this triazole to the surface, which posses higher number of lone pairs from heteroatoms and  $\pi$ -orbitals.

**Table 3.** Corrosion parameters for steel in aqueous solution of 1M HCl in absence and presence of different concentrations of alizarin red from weight loss measurements at 298 K for 6h.

Inhibitor concentration (M)	W <sub>corr</sub> (mg/cm <sup>2</sup> .h)	IE <sub>w</sub> (%)	$\theta$
HCl	1.2614	-	-
10-5	0.4313	65.8	0.658
10-4	0.1866	85.2	0.852
10-3	0.1324	89.5	0.895
10-2	0.0466	96.3	0.963

### 3.3.2. Effect of temperature and activation parameters of inhibition process

Generally, the corrosion rate of steel in acidic solution increase with the rise of temperature. This is due to the decrease of hydrogen evolution overpotential [47]. In order to understand more about the performance of AZR with the nature of adsorption and activation processes, the effect of temperature is studied. For this purpose, the electrochemical impedance spectroscopy measurements are being employed with the range of temperature 298, 308, 318 and 328 K, for 1 h of immersion, in the absence and presence of  $10^{-2}$ M of inhibitor (Figures 4 and 5). Corresponding data are given in Table 4.

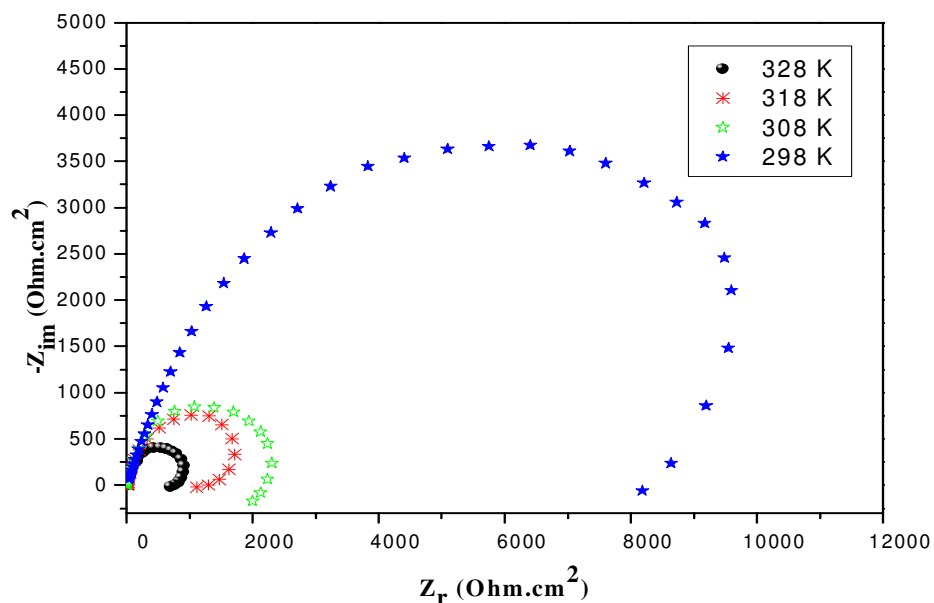


**Figure 4.** Nyquist diagrams for C38 steel in 1 M HCl +  $10^{-2}$  M of Alizarin  $10^{-2}$  M at different temperatures.

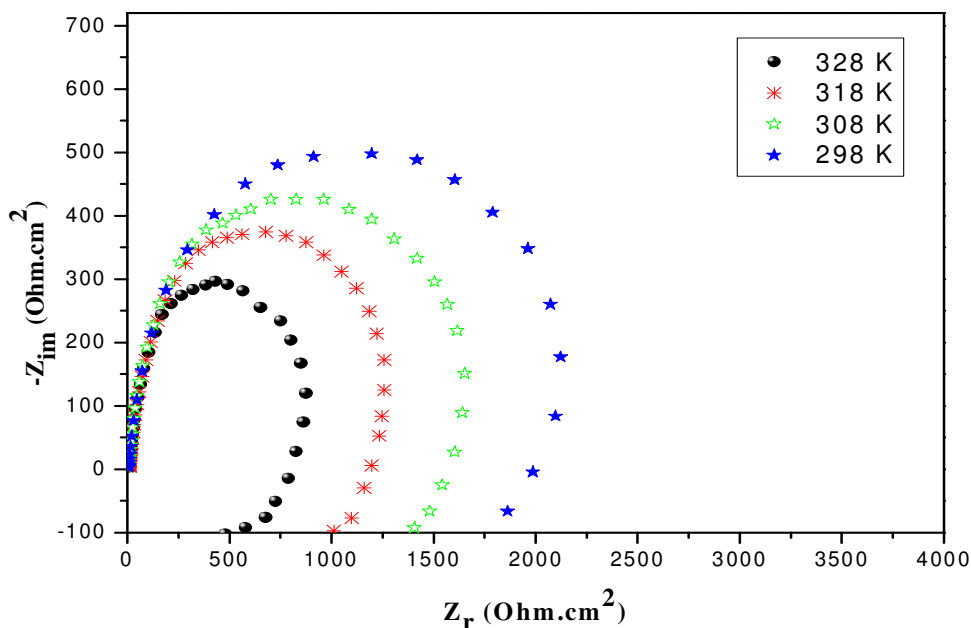


**Figure 5.** Nyquist diagrams for C38 steel in 1 M HCl at different temperatures.

**Table 4.** Thermodynamic parameters for the adsorption of AZR in 1 M HCl on the C38 steel at different temperatures.

Inhibitor	Temp (K)	R <sub>ct</sub> (kΩ.cm <sup>2</sup> )	f <sub>max</sub> (Hz)	C <sub>dl</sub> (ηF/cm <sup>2</sup> )	ER <sub>ct</sub> (%)
1 M HCl	298	10	50	318	-
	308	8	79	251	-
	318	5	100	318	-
	328	4	125	318	-
AZR	298	286	115	4	96.5
	308	60	100	26	86.6
	318	30	79	67	83.3
	328	27	60	98	85.1

The various corrosion parameters obtained are listed in Table 4. The data obtained suggest that AZR get adsorbed on the steel surface at all temperatures studied. Inspection of Table 4 showed that, the temperature rise leads to a decrease of R<sub>ct</sub> values.

As the corrosion rate is inversely proportional to R<sub>ct</sub> values of Ln (1/R<sub>ct</sub>) and Ln (1/R<sub>ct</sub>)/T were plotted as a function of temperature (Arrhenius plots) in Figures 6 and 7 for the corrosion of C38 steel in hydrochloric acid solutions. Values of E<sub>a</sub>, ΔH<sub>a</sub> and ΔS<sub>a</sub> were estimated from the slopes of the straight lines and given in Table 5.

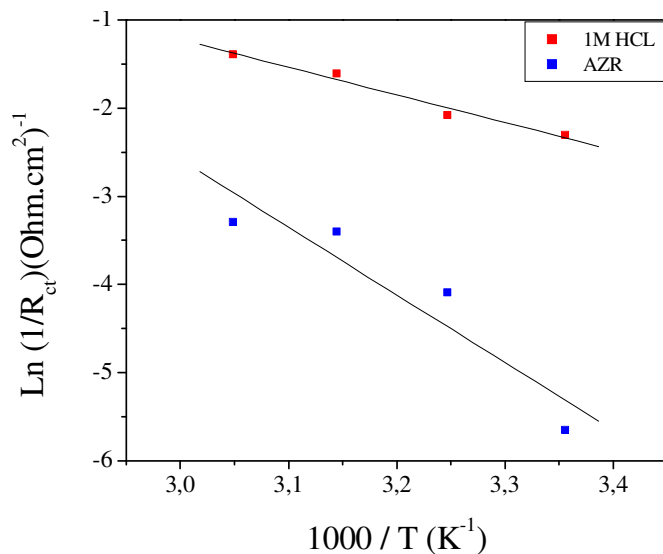


Figure 6. Arrhenius plots Ln 1/R<sub>ct</sub> vs. 1/T of 1 M HCl and 1 M HCl + 10<sup>-2</sup> M of Alizarin red.

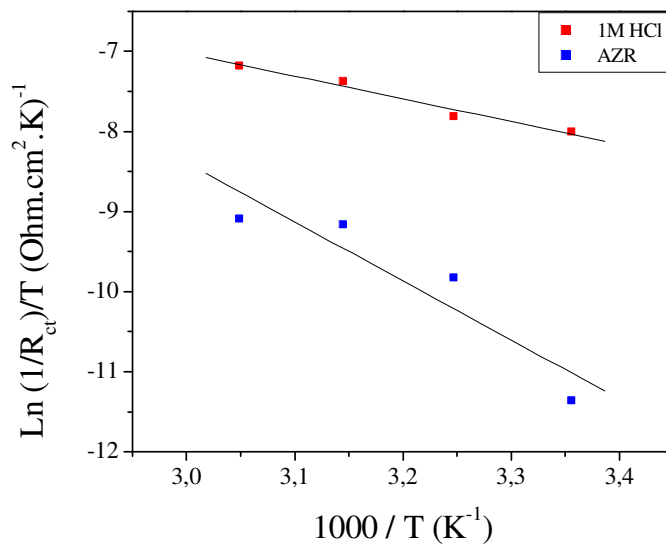


Figure 7. Arrhenius plots of corrosion Ln ((1/R<sub>ct</sub>)/T) vs. 1/T of 1 M HCl and 1 M HCl + 10<sup>-2</sup> M of Alizarin red.

Table 5. The value of activation parameters E<sub>a</sub>, ΔH<sub>a</sub> and ΔS<sub>a</sub> for steel in 1M HCl in the absence and presence of 10<sup>-2</sup> M of alizarin red.

Inhibitor	E <sub>a</sub> (kJ/mol)	ΔH <sub>a</sub> (kJ/mol)	ΔS <sub>a</sub> (J/mol)	E <sub>a</sub> -ΔH <sub>a</sub> (KJ/mol)
Blank	24.55	21.95	-190.65	2.59
AZR	63.85	61.26	-83.38	2.59

Inspection of these data reveals that the  $\Delta H_a$  value for dissolution reaction of carbon steel is higher in the presence of AZR ( $63.85 \text{ kJ mol}^{-1}$ ) than that in its absence ( $24.55 \text{ kJ mol}^{-1}$ ). The positive signs of  $\Delta H_a$  reflect the endothermic nature of the carbon steel dissolution process suggesting that its dissolution is slow in the presence of AZR [48]. One can notice that  $E_a$  and  $\Delta H_a$  values vary in the same way permitting to verify the known thermodynamic reaction between the  $E_a$  and  $\Delta H_a$  as shown in Table 5 [49]:

$$\Delta H_a = E_a - RT \quad (8)$$

Large and negative value of entropic ( $\Delta S_a$ ) imply that the activated complex in the rate determining step represents an association rather than a dissociation step, meaning that a decrease in disordering takes place on going from reactant to the activated complex [50, 51].

### 3.3.3. Adsorption isotherm and adsorption parameters

Adsorption of the organic compound depends upon the charge and the nature of the metal surface, electronic characteristics of the metal surface on adsorption of solvent and other ionic species, temperature of the corrosion reaction and the electrochemical potential at the metal solution interface [52]. Adsorption of the alizarin red involves two types of the possible interaction with the metal surface. The first one is weak undirected interaction due to electrostatic attraction between inhibiting organic ions or dipoles and the electrically charged surface of the metal. This interaction is termed physical adsorption or physisorption. The second type of interaction occurs when there is interaction between the adsorbate and adsorbent. This type of interaction involves charge sharing or charge transfer from adsorbate to the atoms of the metal surface in order to form a coordinate type bond and the interaction is termed chemical adsorption or chemisorptions [53].

Adsorption isotherms are usually used to describe the adsorption process. The most frequently used isotherms include Langmuir, Temkin, Frumkin, Hill deBoer, Parsons, Flory-Huggins, Dhar-Flory-Huggins, Bockris-Swinkels and thermodynamic/kinetic model of El-Awady et.al. [54-56]. The adsorption isotherm provides important clues regarding the nature of the metal-inhibitor interaction. Inhibitor molecules adsorb on the metal surface if the interaction between molecule and metal surface is higher than that of the water molecule and the metal surface [57]. In order to obtain the adsorption isotherm, the degree of surface coverage ( $\Theta$ ) for various concentrations of the inhibitor at 298 K was calculated using equation (7) and listed in the Table 6. Langmuir isotherm was tested for its fit to the experimental data. Langmuir adsorption isotherm is given by following equation [58]:

$$\frac{\Theta}{1-\Theta} = K_{ads} C \quad (8)$$

The rearrangement gives the following equation :

$$\frac{C}{\Theta} = \frac{1}{K_{ads}} + C \quad (9)$$

With

$$K_{ads} = \frac{1}{55.5} \exp\left(\frac{-\Delta G_{ads}^{\circ}}{RT}\right) \quad (9)$$

where  $C_{inh}$  is the inhibitor concentration,  $K_{ads}$  is the adsorption equilibrium constant,  $\Delta G_{ads}^{\circ}$  is the standard free energy of adsorption, 55.5 is the concentration of water in the solution in  $\text{mol dm}^{-3}$ ,  $R$  is the universal gas constant and  $T$  is the absolute temperature in Kelvin.

The thermodynamic parameters from the Langmuir adsorption isotherm are listed in Table 6.

**Table 6.** Thermodynamic parameters for the adsorption of AZR in 1M HCl on the C38 steel at 3298K

Inhibitor	Slope	Kads (M-1)	R2	$\Delta G_{ads}^{\circ}$ (KJ/mol)
AZR	1.03	31423.12	0.99998	-35.61

The plot of  $C_{inh}/\Theta$  vs.  $C$  gives straight line (Figure 7) (correlation > 0.99998), the deviation of the slope from unity (for ideal Langmuir isotherm) can be attributed to the molecular interaction among the adsorbed inhibitor species [59].

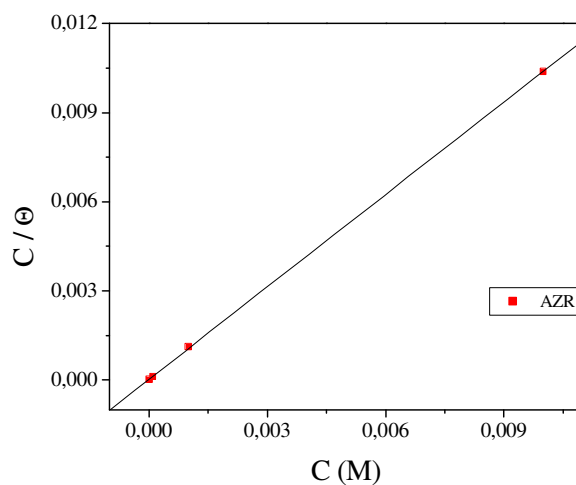


**Figure 7.** Langmuir isotherm adsorption model of AZR on the carbon steel surface in 1M HCl.

From Eq. (9), the  $\Delta G_{ads}^{\circ}$  was calculated as  $-35.61 \text{ kJ mol}^{-1}$ . The negative value of standard free energy of adsorption indicates spontaneous adsorption of AZR molecules on C38 steel surface and also the strong interaction between inhibitor molecules and the metal surface [60, 61]. Generally, the

standard free energy values of  $-20 \text{ kJ mol}^{-1}$  or less negative are associated with an electrostatic interaction between charged molecules and charged metal surface (physical adsorption); those of  $-40 \text{ kJ mol}^{-1}$  or more negative involves charge sharing or transfer from the inhibitor molecules to the metal surface to form a co-ordinate covalent bond (chemical adsorption) [62, 63]. The value of  $\Delta G_{ads}^{\circ}$  in our measurement is  $-35.61 \text{ kJ mol}^{-1}$  (in Table 6), indicating that the adsorption mechanism of AZR on C38 steel in 1M HCl solution at the studied temperature is both electrostatic adsorption (ionic) and chemisorption (molecular) [64].

### 3.4. Quantum chemical calculations

Quantum chemical methods have already proven to be very useful in determining the molecular structure as well as elucidating the electronic structure and reactivity [65]. Thus, it has become a common practice to carry out quantum chemical calculations in corrosion inhibition studies. The predicted properties of reasonable accuracy can be obtained from density functional theory (DFT) calculations [66, 67]. Some quantum chemical parameters, which influence the electronic interaction between surface atoms and inhibitor, are the energy of highest occupied molecular orbital ( $E_{HOMO}$ ), the energy of lowest unoccupied molecular orbital ( $E_{LUMO}$ ), the energy gap  $E_{HOMO} - E_{LUMO}$  ( $\Delta E$ ), dipole moment ( $\mu$ ) and total energy (TE). All quantum chemical properties were obtained after geometric optimization with respect to the all nuclear coordinates using Kohn–Sham approach at DFT level. The optimized structure of the studied compound as shown in Figure 8.

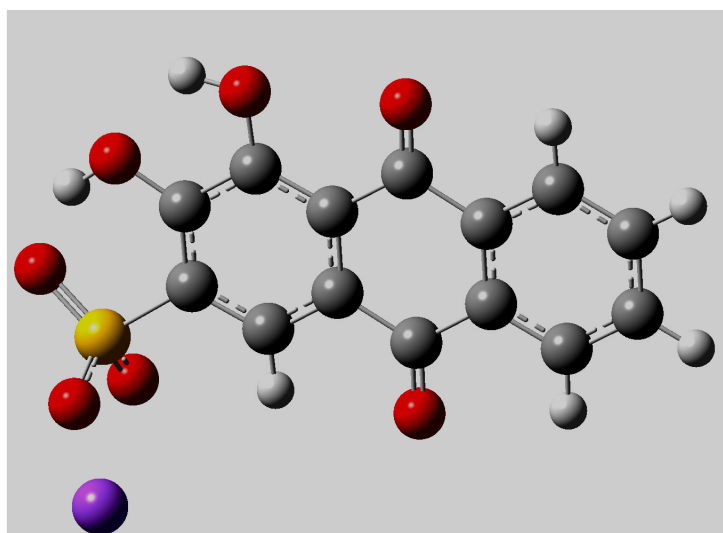


**Figure 8.** Optimized structure of the studied molecule obtained by B3LYP-6-31 G(d) method.

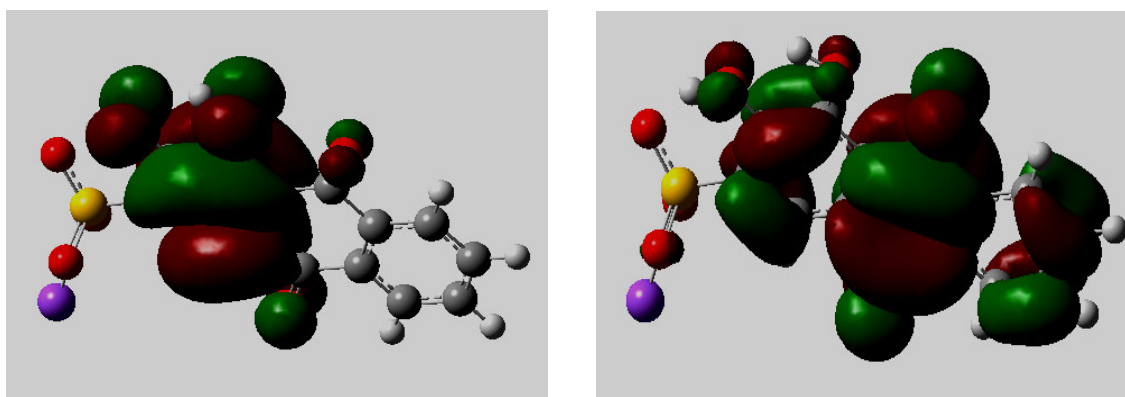
The computed quantum chemical properties such as energy of highest occupied molecular orbital ( $E_{HOMO}$ ), energy of lowest unoccupied molecular orbital ( $E_{LUMO}$ ), HOMO–LUMO energy gap ( $\Delta E_{H-L}$ ), dipole moment ( $\mu$ ) and total energy (TE) are summarized in the Table 7.

**Table 7.** Calculated quantum chemical parameters of studied inhibitor.

Inhibitor	TE (eV)	EHOMO (eV)	ELUMO (eV)	$\Delta E_{\text{gap}}$ (eV)	$\mu$ (Debye)	$\Delta N$ (eV)
AHMT	-44194.3223	-6.081	-2.5228	3.558	8.3346	0.758277

As the energy of HOMO  $E_{\text{HOMO}}$  is often associated with the electron donating ability of a molecule, high values of  $E_{\text{HOMO}}$  are likely to indicate a tendency of the molecule to donate electrons to appropriate acceptor molecules with low-energy, empty molecular orbital. Increasing values of the  $E_{\text{HOMO}}$  facilitate adsorption (and therefore inhibition) by influencing the transport process through the adsorbed layer. Therefore, the energy of the LUMO  $E_{\text{LUMO}}$  indicates the ability of the molecule to accept electrons; hence these are the acceptor states. The lower the value of  $E_{\text{LUMO}}$ , the more probable, it is that the molecule would accept electrons [68]. As for the values of  $\Delta E$  ( $E_{\text{LUMO}} - E_{\text{HOMO}}$ ) concern; lower values of the energy difference  $\Delta E$  will cause higher inhibition efficiency because the energy to remove an electron from the last occupied orbital will be low [69]. On the other hand, the inhibition efficiency increases with the decreasing dipole moment of the inhibitors. As with energetic quantum parameters, some degree of confusion exists when dealing with dipole momentum data interpretation since scientific literature provides both positive [70, 71] as well as negative [72] relationship between this factor and inhibition efficiency. Ju et al. Concluded that physical adsorption results from electrostatic interaction between the charged centers of molecules and charged metal surface, results in a dipole interaction of molecule and metal surface. Therefore, the positive sign of the coefficient of  $\mu$  suggests that these inhibitors can be adsorbed on the alloy surface by physical mechanism.

Frontier orbital theory is useful in predicting the adsorption centers of the inhibitor molecules responsible for the interaction with surface metal atoms [73]. Terms involving the frontier Molecular Orbital could provide dominative contribution, because of the inverse dependence of stabilization energy on orbital energy difference [74]. The high value of  $E_{\text{HOMO}}$  (-6.081 eV) has to indicate a tendency of the molecule to donate electrons to the appropriate acceptor molecules with low energy and empty molecular orbital, whereas the value of  $E_{\text{LUMO}}$  (-2.5228 eV) indicates its ability of the molecule to accept electrons. Consequently, the value of  $\Delta E_{\text{gap}}$  (3.558 eV) provides a measure for the stability of the formed complex on the metal surface [80]. On the other hand, the dipole moment ( $\mu$ ) of the studied compound is 8.3346 Debye, which is higher than that of  $\text{H}_2\text{O}$  ( $\mu = 6.20 \times 10^{-30}$  C.m). The high value of dipole moment probably increases the adsorption between chemical compound and metal surface [75]. Accordingly, the adsorption of our studied molecule from the aqueous solution can be regarded as a quasi-substitution process between the compound in the aqueous phase [AHMT(sol)] and water molecules at the electrode surface [ $\text{H}_2\text{O}(\text{ads})$ ]. In figure 9, we have presented the frontier molecule orbital density distributions of the studied compound: HOMO (right); LUMO (left). Analysis of Figure 9 shows that the distribution of two energies HOMO and LUMO localized in the atoms of the aromatic cycles, consequently this is the favourite sites for interaction with the metal surface. The total energy of is equal to -44194.3223 eV. This result indicated that the Alizarin molecule is favourably adsorbed through the active centers of adsorption.



HOMO

LUMO

**Figure 9.** Frontier molecule orbital density distributions HOMO and LUMO of the studied compound.

#### 4. CONCLUSION

The following conclusions may be drawn from the study:

- Alizarin red (AZR) was found to be a good inhibitor of C38 steel corrosion in hydrochloric acid.
- The inhibition efficiency increases with inhibitor concentration to attain a value of 97.3% ( $10^{-2}$ M) at 298 K.
- The adsorption model obeys to the Langmuir adsorption isotherm.
- Adsorption mechanism of the AZR on C38 steel in a 1M HCl solution at 298K was a combination of both physisorption and chemisorption.
- Polarisation measurements show that AZR acts essentially as a mixed type inhibitor.
- Impedance method indicates that AZR adsorbs on the C38 steel surface with increasing transfer resistance and decreasing of the double-layer capacitance.
- Quantum chemical parameters such as  $E_{\text{HOMO}}$ ,  $E_{\text{LUMO}}$ ,  $\Delta E$  ( $E_{\text{LUMO}} - E_{\text{HOMO}}$ ), dipole moment ( $\mu$ ), number of transferred electrons ( $\Delta N$ ), and total energy (TE) were found to give good correlation with experimentally determined inhibition efficiency.
- The inhibitor efficiency determined by electrochemical polarisation, electrochemical impedance spectroscopy and by gravimetric methods are in good agreement.

#### ACKNOWLEDGEMENTS

Prof S. S. Al-Deyab and Prof B. Hammouti extend their appreciation to the Deanship of Scientific Research at king Saud University for funding the work through the research group project.

#### References

1. S. Ramesh, S. Rajeswari, S. Maruthamuthu, *Mater. Lett.* 57 (2003) 4547.

2. F. Bentiss, F. Gassama, D. Barbry, L. Gengembre, H. Vezin, M. Lagrene'e, M. Traisnel, *Appl. Surf. Sci.* 252 (2006) 2684.
3. M. A. Quraishi, R. Sardar, *Mater. Chem. Phys.* 78 (2003) 425.
4. M. Mihit, L. Bazzi, R. Salghi, B. Hammouti, S. El Issami, E. Ait Addi, *I. S. J. A. E. E.* 62 (6) (2008) 173.
5. B. Hammouti, R. Salghi and S. Kertit, *J. Electrochem Soc. India.* 47 (1998) 31.
6. H. Zarrok, H. Oudda, A. Zarrouk, R. Salghi, B. Hammouti, M. Bouachrine, *Der Pharma Chemica.* 3 (6) (2011) 576.
7. M. Mihit, S. El Issami, M. Bouklah, L. Bazzi, B. Hammouti, E. Ait Addi, R. Salghi, S. Kertit, *Applied Surf. Sci.* 252 (6) (2006) 2389.
8. K. Barouni, L. Bazzi, R. Salghi, M. Mihit, B. Hammouti, A. Albourine, S. El Issami, *Mater. Lett.* 62 (2008) 3325.
9. M. Mihit, R. Salghi, S. El Issami, L. Bazzi, B. Hammouti, E. Ait Addi, S. Kertit, *Pigment & Resin. Tech.* 35 (3) (2006) 151.
10. S. El Issami, L. BAZZI, M. Mihit, M. Hilali, R. Salghi, and E. Ait Addi., *J. Phys. IV*, 123 (2005) 307.
11. S. El Issami, L. Bazzi, M. Hilali, R. Salghi et S. Kertit., *Ann. Chim. Sci. Mat.*, 27(2002) 63–72.
12. S. El Issami, L. Bazzi, M. Mihit, B. Hammouti, S. Kertit, E. Ait Addi, R. Salghi, *Pigment & Resin. Tech.* 36(3) (2007) 161.
13. R. Salghi, L. Bazzi, B. Hammouti and S. Kertit., *Bull. of Electrochem.* 16 (6) (2000) 272.
14. M. Mihit, K. Laarej, H. Abou El Makarim, L. Bazzi, R. Salghi, B. Hammouti, *Arabian J. Chem.* 3 (2010) 55.
15. A. Zarrouk, A. Dafali, B. Hammouti, H. Zarrok, S. Boukhris, M. Zertoubi, *Int. J. Electrochem. Sci.* 5 (2010) 46.
16. A. Zarrouk, T. Chelfi, A. Dafali, B. Hammouti, S.S. Al-Deyab, I. Warad, N. Benchat, M. Zertoubi ; *Int. J. Electrochem. Sci.* 5 (2010) 696.
17. A. Zarrouk, B. Hammouti, A. Dafali, H. Zarrok, *Der Pharma Chemica.* 3 (4) (2011) 266.
18. A. Zarrouk, B. Hammouti, R. Touzani, S. S. Al-Deyab, M. Zertoubi, A. Dafali, S. Elkadiri, *Int. J. Electrochem. Sci.* 6 (2011) 4939.
19. A. Zarrouk, B. Hammouti, H. Zarrok, *Der Pharma Chemica*, 3 (5) (2011) 263-271.
20. H. Zarrok, R. Saddik, H. Oudda, B. Hammouti, A. El Midaoui, A. Zarrouk, N. Benchat, M. Ebn Touhami, *Der Pharma Chemica*, 3 (5) (2011) 272.
21. A. Zarrouk, B. Hammouti, A. Dafali, H. Zarrok, R. Touzani, M. Bouachrine, M. Zertoubi, *Res. Chem. Intermed.* (2011) DOI 10.1007/s11164-011-0444-2.
22. A. Zarrouk, B. Hammouti, H. Zarrok, M. Bouachrine, K.F. Khaled, S.S. Al-Deyab, *Int. J. Electrochem. Sci.* 6 (2012) 89.
23. Shuduan Deng, Xianghong Li, Hui Fu, *Corros. Sci.* 53 (2011) 3596.
24. H. Zarrok, R. Salghi, A. Zarrouk, B. Hammouti, H. Oudda, Lh. Bazzi, L. Bammou, S. S. Al-Deyab, *Der Pharma Chemica.* 4 (1) (2012) 407.
25. E.E. Ebenso, H. Alemu, S.A. Umoren, I.B. .Obot, *Int. J. Electrochem. Sci.* 4 (2008) 1325.
26. A. D. Becke, *J. Chem. Phys.* 96 (1992) 9489.
27. A. D. Becke, *J. Chem. Phys.* 98 (1993) 1372.
28. C. Lee, W. Yang, R.G. Parr, *Phys. Rev. B.* 37 (1988) 785.
29. Gaussian 03, Revision B.01, M. J. Frisch, et al., Gaussian, Inc., Pittsburgh, PA, 2003.
30. M. Bouklah, N. Benchat, A. Aouniti, B. Hammouti, M. Benkaddour, M. Lagrenee, H. Vezin, F. Bentiss, *Prog. Org. Coat.* 51 (2004) 118.
31. M. S. Morad, A. M. K. El-Dean, *Corros. Sci.* 48 (2006) 3398.
32. K. Tebbji, B. Hammouti, H. Oudda, A. Ramdani, M. Benkadour, *Appl. Surf. Sci.* 252 (2005) 1378.
33. A. Yurt, A. Balaban, S. Ustun Kandemir, G. Bereket, B. Erk, *Mater. Chem. Phys.* 85 (2004) 420.
34. B.G. Ateya, M.B.A. El-Khair, I.A. Abdel-Hamed, *Corros. Sci.* 16 (1976) 163.

35. Y. Abboud, A. Abourriche, T. Saffaj, M. Berrada, M. Charrouf, *Appl. Surf. Sci.* 252 (2006) 8178.
36. E. McCafferty, N. Hackerman, *J. Electrochem. Soc.* 119 (1972) 146.
37. W.J. Lorenz, F. Mansfeld, *Corros. Sci.* 21 (1981) 647.
38. F. Bentiss, M. Bouanis, B. Mernari, M. Traisnel, H. Vezin, M. Lagrenee, *Appl. Surf. Sci.* 253 (2007) 3696.
39. A. A. Aksut, W.J. Lorenz, F. Mansfeld, *Corros. Sci.* 22 (1982) 611.
40. A. Caprani, I Epelboin, P. Morel, and H. Takenouti, Proceedings of the 4th European sym. on Corros. Inhibitors, Ferrara, Italy (1975) 571.
41. J -Bessone, C. Mayer, K. Tuttner, and W. J. Lorenz, *Electrochim. Acta.* 28 (1983) 171.
42. F. Bentiss, M. Traisnel and M. Lagrenee, *Corros. Sci.* 42 (2000) 127.
43. S. Murlidharan, K.L.N. Phani, S. Pitchumani and S. Ravichandran, *J. Electrochem. Soc.* 142 (1995) 1478.
44. S. S. Abdel Rehim, O. A. Hazzazi, M.A. Amin and F.K. Khaled, *Corros. Sci.* 50 (2008) 2258
45. H. Ashassi Sorkhabi, D. Seifzadeh and M.G. Hosseini, *Corros. Sci.* 50 (2008) 3363
46. S. R. Lodha, *Pharmaceutical Reviews.* 6 (2008) 1.
47. A. Popova, E. Sokolova, S. Raicheva, M. Christov, *Corros. Sci.* 45 (2003) 33.
48. N.M. Guan, L. Xueming, L. Fei, *Mater. Chem. Phys.* 86 (2004) 59.
49. L. Herrag, B. Hammouti, S. Elkadiri, A. Aouniti, C. Jama, H. Vezin, F. Bentiss, *Corros. Sci.* 52 (2010) 3042.
50. N. Soltani, M. Behpour, S. M. Ghoreishi, H. Naeimi, *Corros. Sci.* 52 (2010) 1351.
51. M. K. Gomma, M. H.Wahdan, *Mater. Chem. Phys.* 39 (1995) 209.
52. R. F. V. Villamil, P. Corio, S. M. L. Agostinho, J. C. Rubin, *J. Electroanal. Chem.* 472 (1999) 112.
53. G. TrabANELLI, in: Mansfeld F (Ed.), Corrosion mechanism, Mercel Dekker, New York, 2006.
54. E. McCafferty in: Leidheiser Jr. H (Ed.), Corrosion control by coating, Science Press, Princeton, 1979
55. E. Khamis, *Corrosion.* 46 (1990) 476.
56. S. S. Abd El-Rehim, A. Magdy, A.M. Ibrahim, K.F. Khaled, *J. Appl. Electrochem.* 29 (1999) 593.
57. G. Moretti, G. Quartarone, A. Tassan, A. Zingales, *Mater. Corros.* 45 (1994) 641.
58. S. Bilgic, N. Caliskan, *Appl. Surf. Sci.* 152 (1999) 107.
59. N.M. Guan, L. Xueming, L. Fei, *Mater. Chem. Phys.* 86 (2004) 59.
60. G. Avci, *Mater. Chem. Phys.* 112 (2008) 234.
61. E. Bayol, A.A. Gurten, M. Dursun, K. Kayakırlmaz, *Acta Phys. Chim. Sin.* 24 (2008) 2236.
62. O. K. Abiola, N.C. Oforka, *Mater. Chem. Phys.* 83 (2004) 315.
63. M. Ozcan, R. Solmaz, G. Kardas, I. Dehri, *Colloid Surf. A.* 325 (2008) 57.
64. S.A. Ali, H.A. Al-Muallem, M.T. Saeed, S.U. Rahman, *Corros. Sci.* 50 (2008) 664.
65. E. Kraka, D. Cremer, *J. Am. Chem. Soc.* 122 (2000) 8245.
66. C. Adamo, V. Barone, *Chem. Phys. Lett.* 330 (2000) 152.
67. M. Parac, S. Grimme, *J. Phys. Chem. A.* 106 (2003) 6844.
68. Z. Zhou, R.G. Parr, *J. Am. Chem. Soc.* 112 (1990) 5720.
69. K.F. Khaled, *Appl. Surf. Sci.* 255 (2008) 1811.
70. A. Stoyanova, G. Petkova, S.D. Peyerimhoff, *Chem. Phys.* 279 (2002) 1.
71. O. Benali, L. Larabi, M. Traisnel, L. Gengembre, Y. Harek, *Appl. Surf. Sci.* 253 (2007) 6130.
72. I.B. Obot, N.O. Obi-Egbedi, S.A. Umoren, *Corros. Sci.* 51 (2009) 276.
73. K. F. Khaled, M.M. Al-Qahtani, *Mater. Chem. Phys.* 113 (2009) 150.
74. J. Fang, J. Li, *J. Mol. Struct. THEOCHEM.* 593 (2002) 179.
75. K. Ramji, D.R. Cairns, S. Rajeswari, *Appl. Surf. Sci.* 254 (2008) 4483